INTERNATIONAL JOURNAL FOR NUMERICAL METHODS IN FLUIDS
Int. J. Numer. Meth. Fluids 2005; **48**:985–1000
Published online 7 April 2005 in Wiley InterScience (www.interscience.wiley.com). DOI: 10.1002/fld.970

Vortex shedding from a square cylinder in presence of a moving wall

S. Bhattacharyya[1,*,†] and D. K. Maiti[2]

[1]*Department of Mathematics, Indian Institute of Technology, Kharagpur 721302, India*
[2]*Department of Mathematics, Birla Institute of Technology and Science, Pilani 333031, India*

SUMMARY

A numerical study on the flow past a square cylinder placed parallel to a wall, which is moving at the speed of the far field has been made. Flow has been investigated in the laminar Reynolds number (based on the cylinder length) range. We have studied the flow field for different values of the cylinder to wall separation length. The governing unsteady Navier–Stokes equations are discretized through the finite volume method on a staggered grid system. A SIMPLE type of algorithm has been used to compute the discretized equations iteratively. A shear layer of negative vortex generates along the surface of the wall, which influences the vortex shedding behind the cylinder. The flow-field is distinct from the flow in presence of a stationary wall. An alternate vortex shedding occurs for all values of gap height in the unsteady regime of the flow. The strong positive vortex pushes the negative vortex upwards in the wake. The gap flow in the undersurface of the cylinder is strong and the velocity profile overshoots. The cylinder experiences a downward force for certain values of the Reynolds number and gap height. The drag and lift are higher at lower values of the Reynolds number. Copyright © 2005 John Wiley & Sons, Ltd.

1. INTRODUCTION

An understanding of the flow past a bluff body close to a moving ground is important in automobile and aeronautical industries. The moving wall induces a forward flow in the horizontal direction near the wall. This can have distinct influence on the vortex shedding behind a bluff body. Bluff body flow in close proximity of a stationary wall has drawn the interest of several authors in recent years, namely, Bearmen and Zdravkovich [1], Bosch and Rodi [2], Lei *et al*. [3] and Zovatto and Pedrizzetti [4]. The stationary wall induces a shear in the incoming velocity profile and the flow differs from its unbounded counterpart. A shear layer with negative vorticity forms along the stationary wall. This negative vorticity interacts with

*Correspondence to: S. Bhattacharyya, Department of Mathematics, Indian Institute of Technology, Kharagpur 721302, India.
†E-mail: somnath@maths.iitkgp.ernet.in

Contract/grant sponsor: CSIR

Received 5 May 2003
Revised 6 January 2005
Accepted 31 January 2005

the vorticity, which originates from the lower side of the bluff body. It has been found that vortex shedding suppression occurs beyond a critical gap height between the bluff body and the stationary wall [1]. For smaller values of the gap height, the vortex shedding process from the bluff body is different from that of a cylinder placed in a free stream [4].

When the wall is considered to be moving horizontally, the classical boundary layer on the wall is absent and the flow mechanism is different from that of the stationary wall. There are only a small number of theoretical studies published in the open literature. Bearmen [5] reviewed earlier studies on bluff body flows that are relevant to the understanding of vehicle flows. There he predicted that the velocity profile may overshoot in the gap flow between the lower surface of the cylinder and the moving wall. The bluff body close to the moving wall may experience a downward force. Arnal *et al*. [6] numerically studied the flow around a rib in contact with a sliding wall. Arnal *et al*. [6] pointed out that the positive vortex that forms in the downstream lower corner of the rib is much weaker when the downstream wall is fixed than when it is moving. Kumarasamy and Barlow [7] studied the flow over a half-cylinder close to a moving wall. An experimental study for three-dimensional flow with free-stream turbulence past an aerodynamic body placed near a moving ground was conducted by Senior and Zhang [8]. They found that the flow remains symmetric about the centre plane of the diffuser and the suction level at the diffuser inlet continues to rise as the ride height is reduced.

The major aim in improvement of the aerodynamics of a car is to reduce the drag and the downforce. The vortex shedding of longitudinal edges on the afterbody is the major source of aerodynamics drag for a vehicle-like body [9]. The vortex shedding and downforce are influenced by the boundary layer along the ground. The influence of the moving wall on the vortex shedding from a bluff body and the gap flow between the body and the wall when the body is in close proximity to it appears not to have been seriously examined as far as we know. Recently, Jones and Smith [10] made a theoretical study on the gap flow between a car underbody and the moving ground.

In this paper, we numerically studied the flow past a square cylinder, which is placed close to a moving ground. The ground travels at a uniform speed, namely the speed of the oncoming free stream of fluid. The flow has been considered to be two-dimensional and laminar. In reality, the flow around a vehicle-like body is three-dimensional and turbulent. Here, a 2D model is considered as a starting point. The numerical method is based on the finite volume scheme. The influence of the moving ground on vortex shedding process behind the cylinder and the gap flow under the cylinder has been investigated. A negative vortex is attached to the moving wall. Our results show that an alternate vortex shedding occurs for all values of the gap height considered. Flow separates near the moving wall in the downstream and close to the wall a small stagnation region appears behind the vortex pair induced by the cylinder. The gap flow is strong and the velocity profiles overshoot within this region. In the next two sections of this paper, we describe the formulation of the problem in non-dimensional terms followed by computational methodology. Subsequently, the results are presented in Section 4. A conclusion is provided in Section 5.

2. THE FORMULATION

We consider the wall lying along the x-axis. A square cylinder of length A is placed parallel to the ground at a height H from the ground. We consider that the far-field and the wall are

moving along x-axis with a constant speed U and the cylinder is stationary. The velocity field is non-dimensionalized by U and the height of the cylinder A is taken to be the characteristic length scale. Thus, the body at height $y = H/A = L$ occupies the range of x between zero and unity in the frame moving with the body.

The time-dependent, two-dimensional Navier–Stokes equations for a constant fluid property in non-dimensional conservative form are given by

$$\frac{\partial u}{\partial x} + \frac{\partial v}{\partial y} = 0 \tag{1}$$

$$\frac{\partial u}{\partial t} + \frac{\partial u^2}{\partial x} + \frac{\partial uv}{\partial y} = -\frac{\partial p}{\partial x} + \frac{1}{Re}\left(\frac{\partial^2 u}{\partial x^2} + \frac{\partial^2 u}{\partial y^2}\right) \tag{2}$$

$$\frac{\partial v}{\partial t} + \frac{\partial uv}{\partial x} + \frac{\partial v^2}{\partial y} = -\frac{\partial p}{\partial y} + \frac{1}{Re}\left(\frac{\partial^2 v}{\partial x^2} + \frac{\partial^2 v}{\partial y^2}\right) \tag{3}$$

where the dimensionless variables are defined as

$$u = \frac{u^*}{U}, \quad v = \frac{v^*}{U}, \quad x = \frac{x^*}{A}, \quad y = \frac{y^*}{A}, \quad p = \frac{p^*}{\rho U^2}, \quad Re = \frac{UA}{\nu}, \quad t = t^* U/A \tag{4}$$

Here, u and v denote the Cartesian components of velocity, ν is the kinematic viscosity, ρ is the fluid density and $L = H/A$ is the non-dimensional gap height from the cylinder to the moving wall.

At the far upstream, the transverse velocity component is set to zero, and horizontal velocity component is assumed to be unity. At the moving wall and cylinder surface, no-slip boundary conditions are applied:

$$u = v = 0 \quad \text{on the cylinder} \tag{5}$$

$$u = 1, \; v = 0 \quad \text{on the moving wall } y = 0 \tag{6}$$

Further,

$$u \to 1, \; v \to 0 \quad \text{in the upstream} \tag{7}$$

A zero-gradient boundary condition is applied at the outflow boundary, and a symmetry boundary condition is prescribed on the top lateral boundary. Flow is assumed to start from rest impulsively.

3. NUMERICAL METHOD AND ALGORITHM TESTING

We used the pressure correction based iterative algorithm SIMPLE [11] for solving the governing equations with those boundary conditions specified previously. The computational domain is divided into Cartesian cells. Staggered grid arrangements (Figure 1(a)) are used in which velocity components are stored at the midpoints of the cell sides to which they are normal. The pressure is stored at the centre of the cell. A first-order implicit scheme is used for time derivatives discretization. However, we have tested our algorithm with three-time step implicit

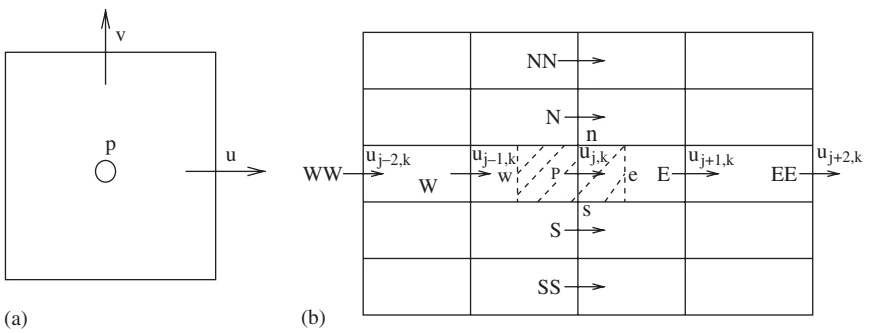

Figure 1. Schematic of: (a) p-control volume; and (b) u-control volume.

scheme to discretize the time derivatives. A detailed discussion has been made later in this section.

The u-momentum equation after integration over the u-control volume (Figure 1(b)) becomes

$$F_e u_e - F_w u_w + F_n u_n - F_s u_s = b \tag{8}$$

where F_e is the non-linear coefficient of u_e. b contains the source terms, diffusion terms and time-derivative terms. The convective terms at any interface are estimated by a linear extrapolation of the u_e values at two upwind neighbours, thus

$$F_e u_e = (\tfrac{3}{2} u_P - \tfrac{1}{2} u_W)[[F_e, 0]] - (\tfrac{3}{2} u_E - \tfrac{1}{2} u_{EE})[[-F_e, 0]] \tag{9}$$

The v-momentum equation has been discretized in a similar manner. This upwind scheme is discussed in detail by Thakur and Shy [12]. The diffusion terms at any interface are estimated by a linear interpolation between two grid point neighbours on either side of the interface. The pressure link between continuity and momentum is accomplished by transforming the continuity equation into a Poisson equation for pressure. The Poisson equation implements a pressure correction for a divergent velocity field.

A single iteration consists of the following sequential steps:

1. An implicit calculation of the u, v momentum equation is performed.
2. The Poisson equation for pressure correction is solved using the successive under-relaxation method. In this case the under-relaxation factor is chosen as 0.975.
3. The velocity field at each cell is updated using the pressure correction.

Iterations at each time step continue until the divergence-free velocity field is obtained. However for this purpose, the divergence in each cell is towed below a preassigned small quantity (ε). In the present case ε is 0.5×10^{-4}. At the initial stage, the number of iterations to converge is about 200 but after the transient state it takes a lesser number of iterations at each time step.

A time-dependent numerical solution is achieved by advancing the flow field variables through a sequence of short time steps of duration δt. At the initial stage of motion the time step δt is taken to be 0.001, which has been subsequently increased to 0.005 after the transient state. Further change in time step does not produce any significant change in the solution.

In order to achieve a higher accuracy in time derivative discretization, we have employed a second-order accurate implicit scheme. This scheme involves a backward difference in time. For the choice of δt indicated before, the difference in solution between the Euler implicit scheme and three-time level implicit scheme is found to be insignificant (see Figures 4 and 9). The maximum percentage difference is found to be below 0.5%. We also found that the Euler implicit scheme is computationally economical for smaller values of δt as the three-time level implicit scheme requires storage of two previous time step solutions and the computation time is higher. Because of this, we made the computations presented here through the Euler implicit scheme.

The heights of the top lateral boundary and outflow boundary are chosen large enough such that the influence of the boundary condition on the wall shear stress is very weak. Tests were made in order to determine the suitable distances of the top boundary and downstream boundary. The outflow boundary distance is increased with an increase in Re. For a typical computation at $Re = 250$ and $L = 0.25$, for example, the top lateral boundary and outflow boundary are taken as $8A$ from the moving wall and $20A$ from the cylinder rear face, respectively. Further changes in outflow boundary and top lateral boundary distances do not produce any significant change in the results.

A non-uniform grid distribution in the computational domain is incorporated. Figure 2 shows the grid distribution near the cylinder faces and moving wall. The grid is finer near the surfaces of the square cylinder and moving wall to better resolve the gradients near the solid surfaces. To check the grid independency, we performed computations for four set of grids namely: 185×170, 185×340, 370×170 and 370×340 with the first and second number being the number of mesh points in the x-direction and in the y-direction, respectively. The maximum distance of the first grid point from each wall is $0.01A$ and $0.005A$ for the coarse and fine grids, respectively. The effect of grid size on Strouhal number (St) and the time-average drag coefficient ($\overline{C}_D$) experienced by the cylinder at various values of the Reynolds number for uniform flow past a square cylinder placed in an unbounded region is presented in Figures 3(a) and 3(b). We find that the changes in solution due to halving the grid size occur on the third decimal place. The effect of grid refinement on St for the case of moving ground is shown in Figure 4 at various values of the Reynolds number when gap height is 0.5. The changes on St due to halving the grids from 185×170 occur mostly on the third decimal place. The maximum percentage difference of St between solution with grids 185×170 and 370×340 is about 6% at $Re = 1000$. We find that 185×170 grids are optimum at $L = 0.5$. For lower values of gap height, the grid points along the y-direction are slightly reduced.

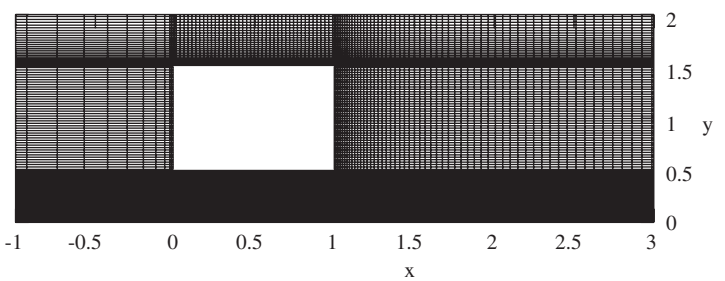

Figure 2. The arrangement of the computational grid in the computational domain near the cylinder faces and moving wall.

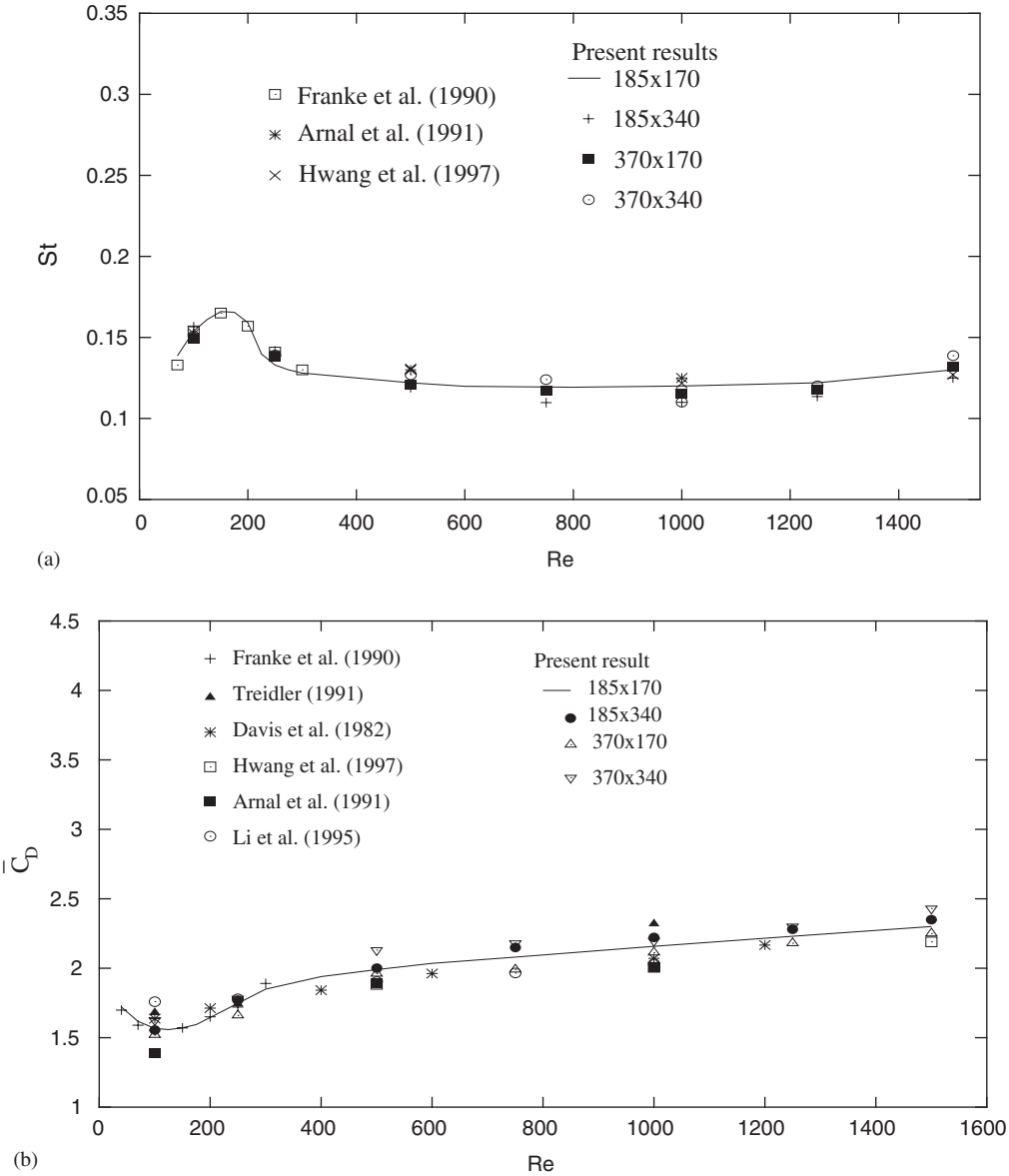

Figure 3. Comparison among: (a) Strouhal number (St); and (b) average drag coefficient ($\overline{C}_D$) results for the flow past a square cylinder in freestream for different grid sizes.

In order to assess the accuracy of our numerical method, we have computed St and $\overline{C}_D$ for uniform flow past a square cylinder without a plane wall at different values of Re and compared with the results due to Davis and Moore [13], Franke *et al.* [14], Treidler [15], Arnal *et al.* [6], Li and Humphrey [16] and Hwang and Yao [17]. Our results are in excellent

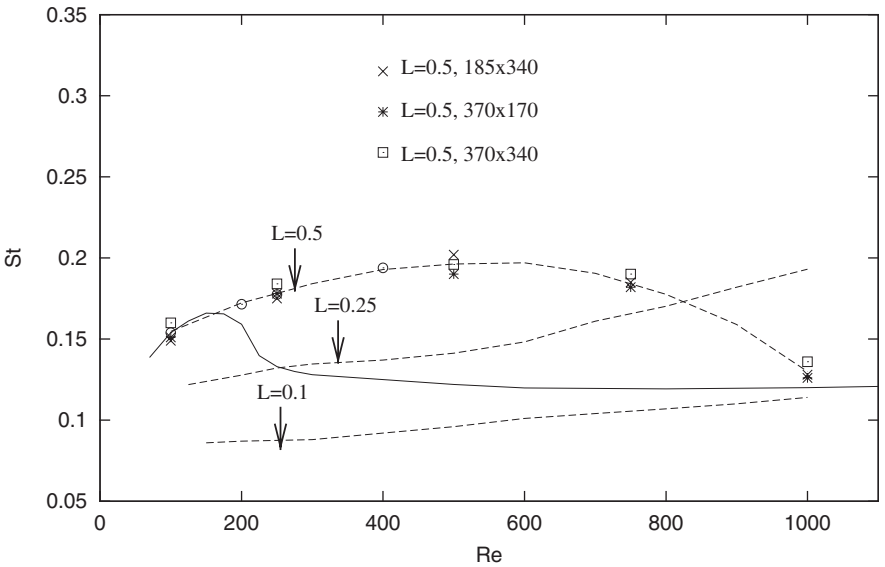

Figure 4. Variation of Strouhal number (St) with Reynolds number (Re) for different gap heights $L = 0.5, 0.25, 0.1$. Solid line: freestream; Dotted line: moving ground; ○: $L = 0.5$, 185×170 using three time step implicit scheme.

agreement with those of Franke *et al.* [14], Arnal *et al.* [6] and Hwang and Yao [17]. The maximum percentage difference of St from the result due to Arnal *et al.* [6] is 4% at $Re = 1000$ and the difference with Hwang and Yao [17] is 2.3% at $Re = 1500$. The maximum difference of our $\overline{C}_D$ with Hwang and Yao [17] at $Re = 1500$ is 5% and about 6% from Arnal *et al.* [6] at $Re = 1000$. Our computed results for $\overline{C}_D$ differences with Li and Humphrey [16] results by 12% and with Arnal *et al.* [6] by 11% at $Re = 100$, but agrees well with Franke *et al.* [14] and Davis and Moore [13]. It may be noted that Li and Humphrey [16] results differ from Arnal *et al.* [6] results at $Re = 100$ by 21%.

4. RESULTS AND DISCUSSIONS

The present flow field is governed by two parameters, namely, the Reynolds number Re and the ground to cylinder gap height L. We have presented the numerical solutions at $L = 0.5, 0.25, 0.1$ for different values of the Reynolds number.

The variation of the Strouhal number (St) with the Reynolds number at various values of cylinder to wall gap height $L = 0.5, 0.25, 0.1$ is presented in Figure 4. A periodic flow field is observed after a short transient flow. The vortex-shedding frequency is determined from the time evolution plot of the lift coefficient distribution. The time period T is the difference between the two successive non-dimensional time at which the lift coefficient attain its minimum value. The time evolution of the lift coefficient (C_L) is described in Figure 5 for $Re = 250$, 500 and 800. The behaviour of the Strouhal number with the Reynolds number is

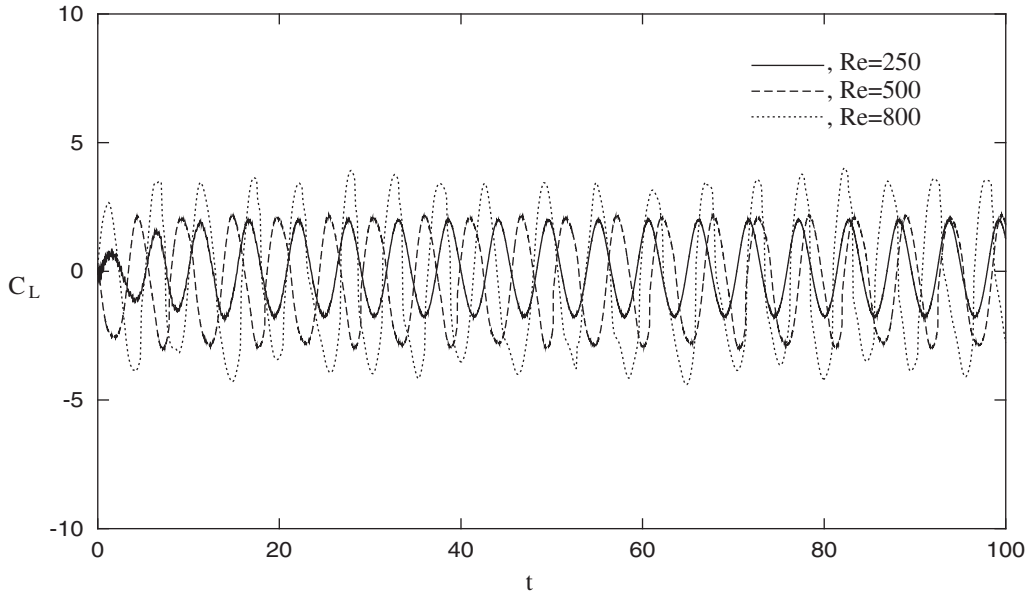

Figure 5. Time evolution of lift coefficient (C_L) for gap height $L = 0.5$ at Reynolds number $Re = 250$, 500 and 800.

not uniform. The periodicity in the frequency of vortex shedding decreases with the decrease in gap height ratio of the cylinder to the wall. The decrease becomes more significant for higher values of Reynolds number. The variation of St with the Reynolds number at gap height $L = 0.1$ is not significant. It has been found that for the present case, the transition from steady flow to a periodic vortex shedding regime occurs at a larger Reynolds number compared to the case where the cylinder is in free stream. The periodic shedding is delayed because the vorticity shed from the cylinder's wall side couples with the wall vorticity, which arrests its evolution. In the unsteady regimes, the vortex shedding pattern is similar to the von Karman vortex street, even if the sliding wall produces a cancellation on the positive vortex emerging from the lower shear layer.

Figure 6 displays the evolution of instantaneous vorticity during a cycle of vortex shedding when $Re = 500$ and $L = 0.5$. In the vicinity of the cylinder and the moving wall, there are three shear layers, the two shear layers that develop along the surface of the cylinder on the top and bottom, respectively, and the shear layer that develops along the wall. The upper shear layer on the cylinder has negative vorticity, while the lower shear layer on the cylinder has positive vorticity. These vortices attain maximum strength before being shed. A shear layer of negative vorticity forms along the moving wall in the downstream of the cylinder. Due to the absence of the classical boundary layer on the moving wall, the secondary vortex strength is greatly reduced compared to the case of a stationary wall. This wall-induced negative vortex interacts with the vortex pair and influences the shedding process.

We find from Figure 6 that an alternate negative and positive vortex shedding occurs behind the cylinder. At the starting of the shedding cycle, where the cylinder experiences the

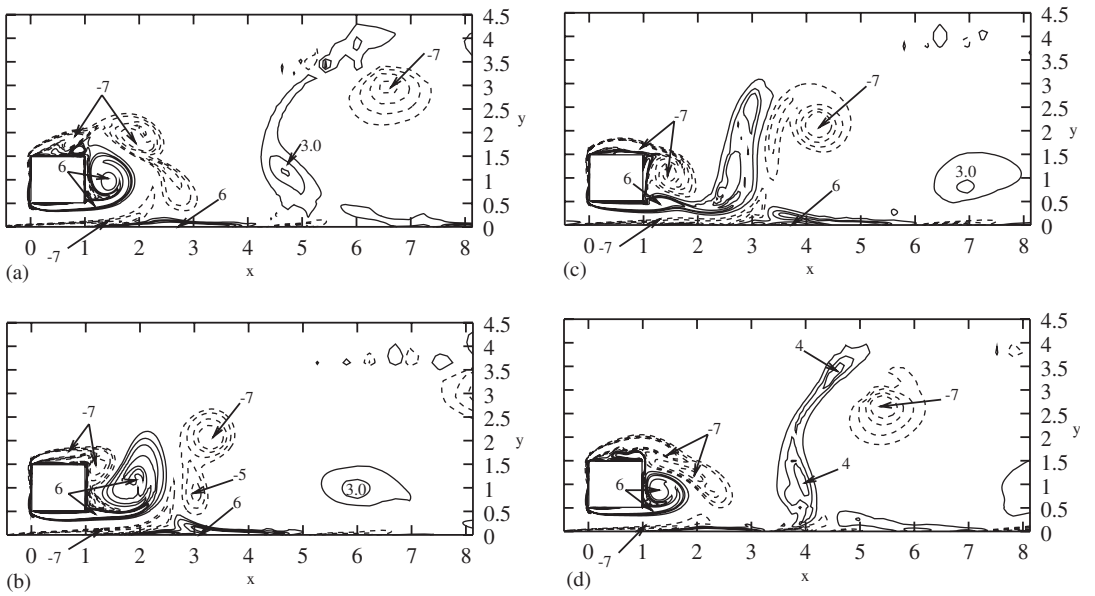

Figure 6. Iso-vorticity contours during one shedding cycle for gap height $L = 0.5$ at $Re = 500$. (a) $t = 60.49$ $(= T)$; (b) $t = 61.748$ $(= T + T/4)$; (c) $t = 63.005$ $(= T + T/2)$; and (d) $t = 64.263$ $(= T + 3T/4)$.

maximum drag, the negative vortex induced at the upper shear layer grows rapidly before being shed. The negative vortex shedding occurs at $t = 61.748$ $(= T + T/4)$ and the positive vortex induced in the lower shear layer grows in size and elongates. At $t = 64.263$ $(= T + 3T/4)$ the positive vortex is shed in the wake. Results show that the positive vortex induced at the lower side of the cylinder is quite strong and the size is much bigger than the case when the cylinder is in the vicinity of a stationary wall. The strong positive vortex induces an upward motion and pushes the negative vortex as it moves downstream. Results also show that the vortex shed from the upper side is nearly circular, while the vortex shed from the lower side is substantially stretched in the local flow direction. The lower shear layer is strongly influenced by the presence of the adjacent wall. The shedding process is similar to the case when the cylinder is placed in a uniform stream. The negative vortex on the wall shear layer grows in size and remains attached to the wall without being shed. Close to the wall, vorticity changes sign further downstream of the cylinder. This indicates that a stagnation region exists near the wall.

The development of wake during one Strouhal shedding period for cylinder to wall gap height ratio $L = 0.5$ at $Re = 500$ is described by presenting the instantaneous streamline patterns in Figure 7 at those time levels where the lift is minimum, zero or maximum. Fluid flowing over the cylinder separates from the front and produces a negative vortex (clockwise rotation). The lower face of the cylinder induces a positive vortex (anticlockwise rotation). Downstream of the cylinder $(x > 2)$, flow separates near the wall and a small region of back flow occurs. This separation appears to be coupled in a periodic manner with vortex shedding from the cylinder. The shedding process is similar to the case of the cylinder in a uniform stream. The

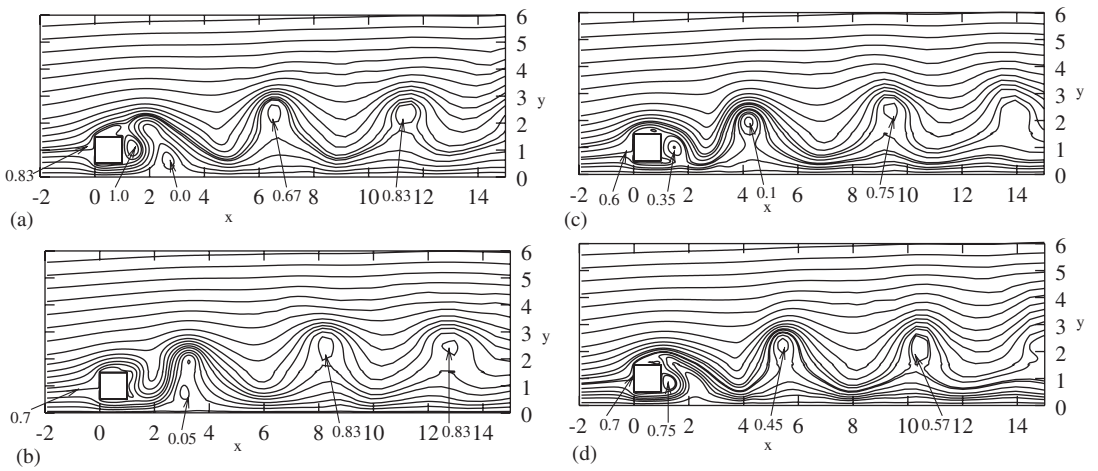

Figure 7. Streamlines during one shedding cycle for gap height $L = 0.5$ at $Re = 500$. (a) $t = 60.49$ $(= T)$; (b) $t = 61.748$ $(= T + T/4)$; (c) $t = 63.005$ $(= T + T/2)$; and (d) $t = 64.263$ $(= T + 3T/4)$.

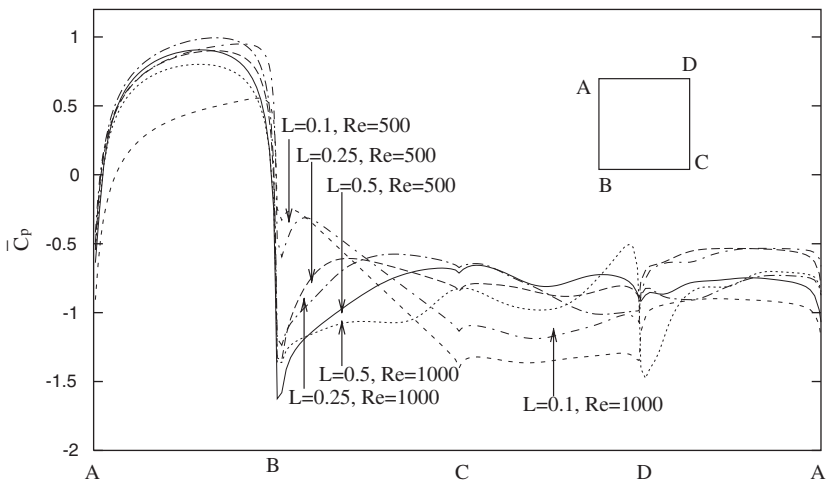

Figure 8. Time-average pressure coefficient $(\overline{C}_p)$ over the cylinder for gap height $L = 0.5, 0.25, 0.1$ at $Re = 500, 1000$.

formation of Karman vortex street and alternate shedding of vortices behind the cylinder is clear from the figures. Fluid impinges on the front of the cylinder and is forced over it. Fluid flowing over the cylinder is forced down behind the cylinder by the growing vortex on the cylinder top surface. This raises the pressure behind the cylinder and, as a result, lowers the drag force acting on it. The lower downstream corner of the cylinder induces an anticlockwise (positive) rotating zone. The size of the anticlockwise rotating zone is much larger than the case when the cylinder is close to a stationary ground. As the positive vortex originating from

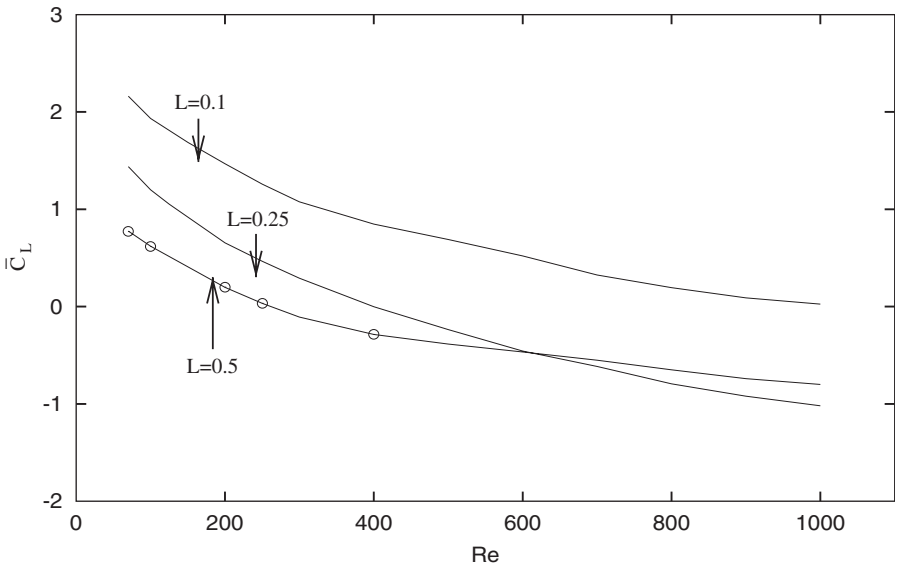

Figure 9. Time-average lift coefficient ($\overline{C}_L$) as a function of Reynolds number (Re) for gap height $L = 0.5, 0.25, 0.1$. $\circ$: $L = 0.5$ using three time step implicit scheme.

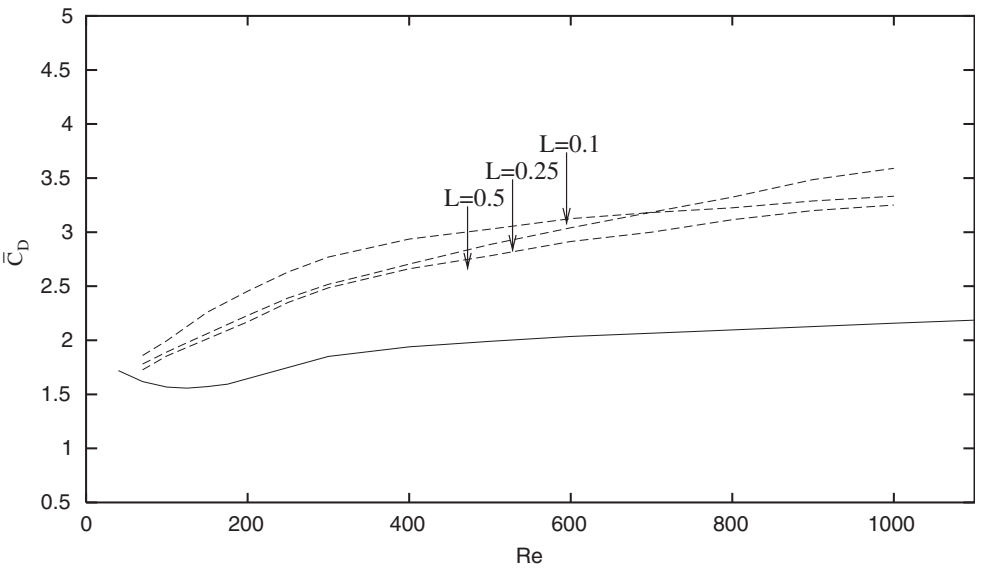

Figure 10. Time-average drag coefficient ($\overline{C}_D$) as a function of Reynolds number (Re) for gap height $L = 0.5, 0.25, 0.1$. Solid line: freestream, Dotted line: moving ground.

the cylinder lower shear layer grows, an upward jet forms between it and the upper layer negative vortex. This jet acts to push fluid back towards the cylinder. A flow recirculation occurs near the wall in the downstream region of the cylinder.

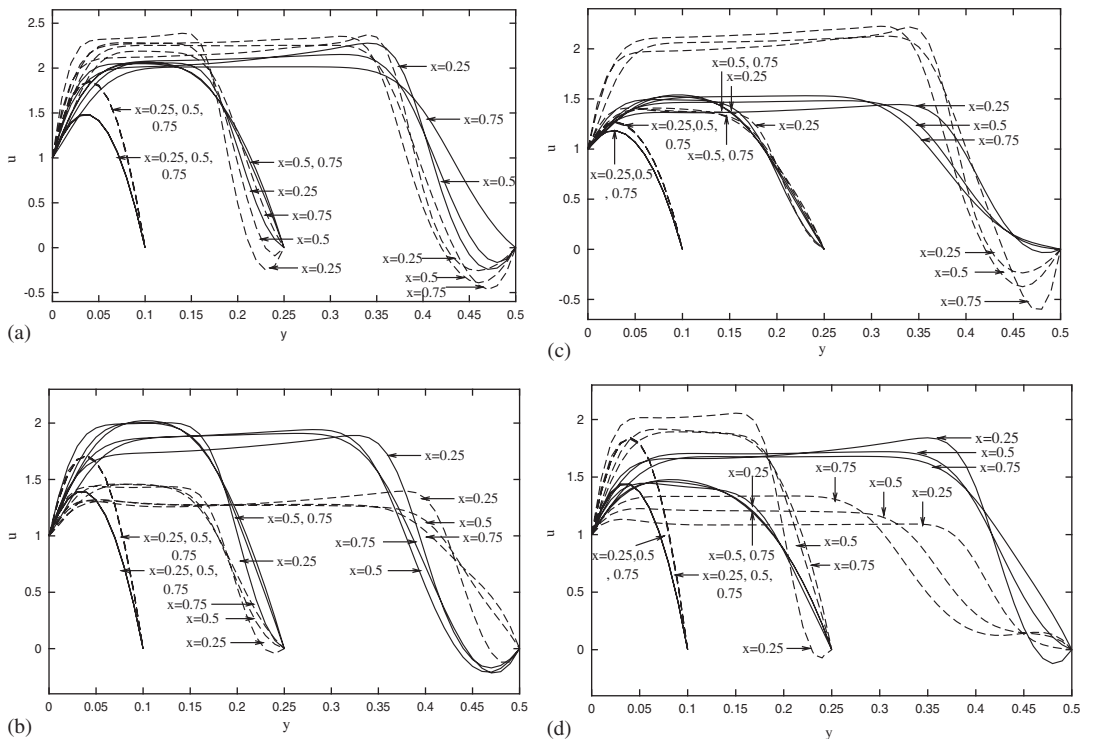

Figure 11. The profiles of the horizontal component of velocity in the gap flow during one shedding cycle for different values of gap height $L = 0.5, 0.25, 0.1$ at $Re = 500, 1000$. (a) $t = T$; (b) $t = T + T/4$; (c) $t = T + T/2$; and (d) $t = T + 3T/4$. Solid line: $Re = 500$, Dotted line: $Re = 1000$.

We have seen (not presented here for the sake of brevity) that vortex shedding occurs even at smaller gap height $L = 0.1$. The streamlines exhibit oscillation and the flow is periodic up to a Reynolds number 1000, while in the case of flow past a bluff body in proximity of a stationary wall, the vortex shedding suppression occurs beyond a critical value of cylinder to wall gap height [1]. For the case of the stationary wall, the jet through the gap between the cylinder and the wall separates near the front lower corner of the cylinder, attaches behind the cylinder surface and does not roll-up to form vortex shedding. The separated upper shear layer of negative vorticity is almost horizontal for the case of stationary wall beyond the critical gap height.

The time average mean pressure distribution $\overline{C}_p$ on the surface of the cylinder at various gap heights $L = 0.1, 0.25, 0.5$ with $Re = 500, 1000$ is described in Figure 8. The pressure is negative on the lower face of the cylinder with a suction $(-\overline{C}_p)$ peak to develop at the front of the undersurface. The position of the suction peak shifted slightly with the increase in Re. It is clear from the figure that as the fluid enters the gap region it encounters an adverse pressure gradient for large values of L, whereas the fluid moves with a favourable pressure gradient in the gap region for lower values of L.

The average lift experienced by the cylinder at different Reynolds numbers is illustrated in Figure 9 for $L = 0.1, 0.25, 0.5$. The lift takes positive or negative values depending on the

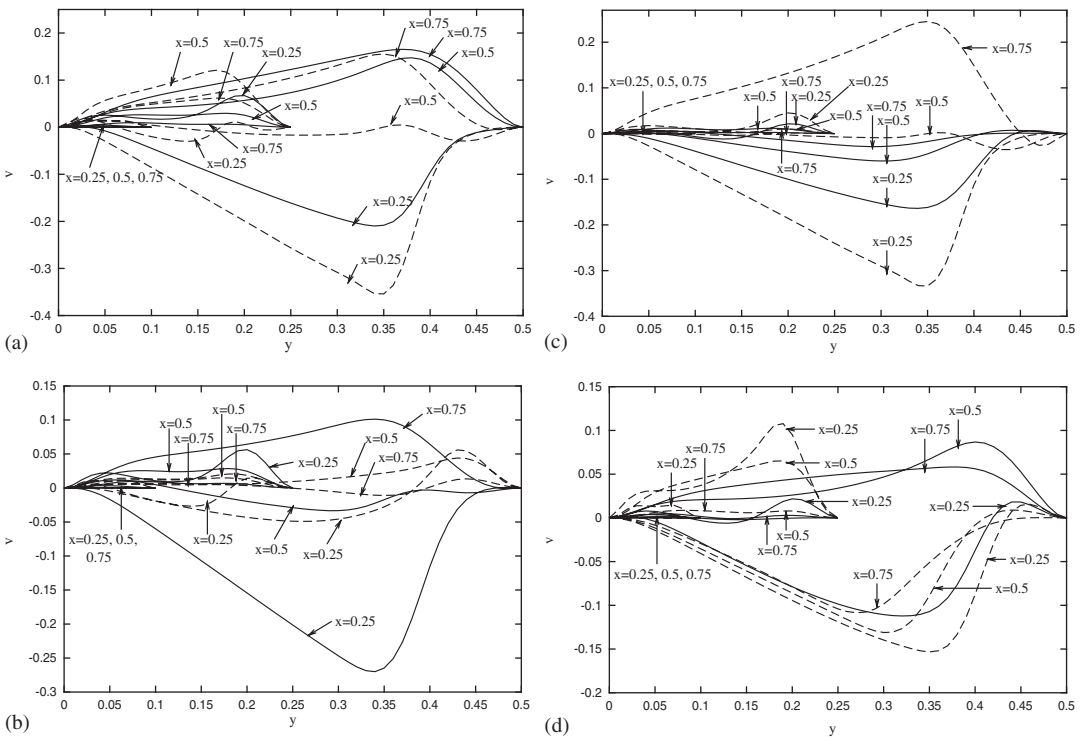

Figure 12. The profiles of the vertical component of velocity in the gap flow during one shedding cycle for different values of gap height $L = 0.5, 0.25, 0.1$ at $Re = 500, 1000$. (a) $t = T$; (b) $t = T + T/4$; (c) $t = T + T/2$; and (d) $t = T + 3T/4$. Solid line: $Re = 500$, Dotted line: $Re = 1000$.

values of the Reynolds number and gap height. The lift experienced by the cylinder decreases as the Reynolds number increases. The lift due to pressure is found to be negative, while the lift due to friction is positive. At low Re, the frictional lift is greater than the pressure lift, whereas the opposite behaviour was seen at higher Re. The cylinder placed near a moving wall experiences a positive lift if in the gap flow a viscous effect dominates. Our results show that the lift is positive for lower values of Reynolds number. At a lower value of gap height ($L = 0.1$) the lift is positive for the entire range of the Reynolds number. For smaller values of gap height, the lubrication effect due to viscosity plays a major role.

Figure 10 shows the average drag coefficient $\overline{C}_D$ at different Re for $L = 0.5, 0.25, 0.1$. The instantaneous drag coefficient is averaged over the shedding cycle to obtain the $\overline{C}_D$. In the case of the cylinder placed in a free stream, the average drag coefficient increases monotonically with the increase in the Reynolds number. In this case, for flow past a cylinder close to a moving wall, the monotonicity of the drag coefficient with the Reynolds number is absent. Due to the presence of the wall shear layer, the drag coefficient is changed greatly. The effect due to the variation of the gap height on the average drag coefficient is small.

The flow under the cylinder is described in Figures 11 and 12 at different values of Reynolds number and cylinder to ground gap height ratio L. We presented the velocity profiles during one period of vortex shedding. A positive surface vorticity on the cylinder's lower face

produces a forward flow in the gap flow occurring in the region under the cylinder and the moving ground. In the present moving frame, the negative surface vorticity near the ground corresponds to an overshoot in velocity profile. The profile of the horizontal component of velocity in the gap flow is shown at different x-station at $Re = 500, 1000$. The horizontal velocity component is positive and overshoots near the moving ground. It may be noted that in a frame fixed in the ground, the local fluid motion is temporarily in the opposite direction (rightwards) from that of the (leftwards moving) body. The profile of vertical component of velocity in Figure 12 shows that the flow is downward near the entry region of the gap and vertical velocity component is positive as we move away from the entry region. Our results show that the fluid slows down relative to the ground velocity as the gap narrows. The fluid velocity increases with the rise of Re. At small gap height, the gap flow is dominated by viscous effect and the u-velocity profile is near parabolic.

5. CONCLUSIONS

The flow past a square cylinder in the vicinity of a moving wall is considered in the above study. The two-dimensional laminar flow is studied for different values of cylinder to wall gap height and the Reynolds number. The characteristics of the wake differ from the corresponding unbounded case and the case in which the bluff body is in close proximity to the stationary wall. A weak shear layer of negative vorticity induced by the moving wall influences the vortex shedding behind the cylinder. The shedding frequency reduces with the reduction in wall to cylinder gap height. But unlike the flow in presence of the stationary wall, here vortex shedding suppression does not occur even at $L = 0.1$. Flow separates from the moving wall in the downstream region of the cylinder. The lift experienced by the cylinder is downwards and is lessened with the increase in the Reynolds number. The drag experienced by the cylinder does not vary much at large Reynolds number for those values of gap height considered in the present study. We find that at $L = 0.5$ and 0.25 the base suction peak occurs near the leading edge of the wall side face of the cylinder. The horizontal component of the velocity overshoots in the gap flow region but no back flow occurs. At the gap height 0.1, the gap flow is almost uni-directional and the gap flow is dominated by viscous force. The flow characteristics in the gap region between the cylinder and the wall agree qualitatively well with the theoretical results due to Jones and Smith [10].

Certain issues were not covered by the present study, e.g. the three-dimensional aspects and turbulence. The three-dimensional features of the vortex stretching due to the wall induced negative vortex will be interesting. The three-dimensional nature of turbulent vortex shedding from a square cylinder in the vicinity of a fixed wall has been investigated by Bailey *et al.* [18]. There they concluded that the vortex formation process is increasingly two-dimensional when the body is close to the wall. There have been several studies on the wake structure and aerodynamic drag reduction for vehicle-like bodies [9, 19]. Those studies and the references there-in provide several results based on either PIV measurement or direct computation of three-dimensional Navier–Stokes equations with k–ε turbulence model. The flow field at those ranges of the Reynolds number is relatively insensitive to the variation of the Reynolds number. The interaction of unsteady flow separation from the moving wall with the wake has not been addressed in those previous studies. The shape of the lower surface of the body has direct impact on the vortex structure and the base pressure.

NOMENCLATURE

A	height of the square cylinder
C_L	lift coefficient
$\overline{C}_L$	time-averaged lift coefficient
$\overline{C}_D$	time-averaged drag coefficient
$\overline{C}_p$	time-averaged pressure coefficient
f	frequency of vortex shedding
H	gap height from cylinder to the moving wall
L	non-dimensional gap height from cylinder to the moving wall, H/A
p	non-dimensionless pressure, $p^*/\rho U^2$
Re	Reynolds number, UA/v
St	Strouhal number, fA/U
T	period of vortex shedding
t	non-dimensional time, t^*U/A
U	reference horizontal velocity
u	dimensionless x-component of velocity, u^*/U
v	dimensionless y-component of velocity, v^*/U
x	dimensionless horizontal distance, x^*/A
y	dimensionless vertical distance, y^*/A

Greek letters

v	kinematic viscosity coefficient
ρ	fluid density

Superscript

$*$	dimensional quantity

ACKNOWLEDGEMENT

The work was financially supported by CSIR through a project grant.

REFERENCES

1. Bearmen PW, Zdravkovich MM. Flow around a circular cylinder near a plane boundary. *Journal of Fluid Mechanics* 1978; **89**:33–47.
2. Bosch G, Rodi W. Simulation of vortex shedding past a square cylinder near a wall. *International Journal of Heat and Fluid Flow* 1996; **17**:267–275.
3. Lei C, Cheng L, Kavanagh K. Re-examination of the effect of a plane boundary on force and vortex shedding of a circular cylinder. *Journal of Wind Engineering and Industrial Aerodynamics* 1999; **80**:263–286.
4. Zovatto L, Pedrizzetti G. Flow about a circular cylinder between parallel walls. *Journal of Fluid Mechanics* 2001; **440**:1–25.
5. Bearmen PW. Review-bluff body flows applicable to vehicle aerodynamics. *Journal of Fluids Engineering* 1980; **102**:265–274.
6. Arnal MP, Georing DJ, Humphrey JAC. Vortex shedding from a bluff body adjacent to a plane sliding wall. *Journal of Fluids Engineering* 1991; **113**:384–398.
7. Kumarasamy S, Barlow JB. Computation of unsteady flow over a half-cylinder close to a moving wall. *Journal of Wind Engineering and Industrial Aerodynamics* 1997; **69–71**:239–248.

8. Senior AE, Zhang X. The force and pressure of a diffuser-equipped bluff body in ground effect. *Journal of Fluids Engineering* 2001; **123**:105–111.
9. Grorche FR, Meier GPA. Research at DLR Gottingen on bluff body aerodynamics, drag reduction by wake ventrilation and achieve flow control. *Journal of Wind Engineering and Industrial Aerodynamics* 2001; **89**:1201–1218.
10. Jones MA, Smith FT. Fluid motion for car undertrays in ground effect. *Journal of Engineering Mathematics* 2003; **45**:309–334.
11. Patankar SV. *Numerical Heat Transfer and Fluid Flow*. Hemisphere Publishing Corporation: Taylor & Francis Group, New York, 1980.
12. Thakur S, Shy W. Some implementational issue of convection schemes for finite-volume formulation. *Numerical Heat Transfer Part B* 1993; **24**:31–55.
13. Davis RW, Moore EF. A numerical study of vortex shedding from rectangles. *Journal of Fluid Mechanics* 1982; **116**:475–506.
14. Franke R, Rodi W, Schonung B. Numerical calculation of laminar vortex shedding flow past cylinders. *Journal of Wind Engineering and Industrial Aerodynamics* 1990; **35**:237–257.
15. Treidler EB. An experimental and numerical investigation of flow past ribs in a channel. *Ph.D. Thesis*, University of California at Berkeley, Berkeley, CA, 1991.
16. Li G, Humphrey JAC. Numerical modelling of confined flow past a cylinder of a square cross-section at various orientation. *International Journal for Numerical Methods in Fluids* 1995; **20**:1215–1236.
17. Hwang RR, Yao C. A numerical study of vortex shedding from a square cylinder with ground effect. *Journal of Fluids Engineering* 1997; **119**:512–518.
18. Bailey SCCR, Martinuzzi RJ, Kopp GA. The effect of wall proximity on vortex shedding from a square cylinder: three-dimensional effects. *Physics of Fluids* 2002; **14**:4160–4176.
19. Muyl F, Dumas L, Herbert V. Hybrid method for aerodynamic shape optimization in automotive industry. *Computers and Fluids* 2004; **33**:849–858.

